

# An Adaptive MHD Method for Global Space Weather Simulations

Darren L. De Zeeuw, Tamas I. Gombosi, Clinto P. T. Groth, Kenneth G. Powell, and Quentin F. Stout

*Invited Paper*

**Abstract**—A 3-D parallel adaptive mesh refinement (AMR) scheme is described for solving the partial-differential equations governing ideal magnetohydrodynamic (MHD) flows. This new algorithm adopts a cell-centered upwind finite-volume discretization procedure and uses limited solution reconstruction, approximate Riemann solvers, and explicit multi-stage time stepping to solve the MHD equations in divergence form, providing a combination of high solution accuracy and computational robustness across a large range in the plasma  $\beta$  ( $\beta$  is the ratio of thermal and magnetic pressures). The data structure naturally lends itself to domain decomposition, thereby enabling efficient and scalable implementations on massively parallel supercomputers. Numerical results for MHD simulations of magnetospheric plasma flows are described to demonstrate the validity and capabilities of the approach for space weather applications.

**Index Terms**—Adaptive mesh refinement, magnetohydrodynamics, numerical simulations, space weather.

## I. INTRODUCTION

SPACE weather is of growing importance to the scientific community and refers to conditions at a particular place and time on the Sun and in the solar wind, magnetosphere, ionosphere, and thermosphere that can influence the performance and reliability of space-borne and ground-based technological systems, and can affect human life or health. It has been established that adverse conditions in the space environment can cause disruption of satellite operations, communications, navigation, and of electric power distribution grids, thereby leading to broad socioeconomic losses. These influences on the geospace environment have prompted renewed efforts to enhance our understanding of space weather and develop effective tools for space weather prediction.

Manuscript received January 15, 2000; revised April 20, 2000. This research was supported by the NSF-NASA-AFOSR interagency Grant NSF ATM-9318181, by the NASA HPC Computational Grand Challenge cooperative agreement Award CAN NCCS5-146 and by the NSF KDI Grant ATM-9980078.

D. L. De Zeeuw and T. I. Gombosi are with the Space Physics Research Laboratory, Department of Atmospheric, Oceanic and Space Sciences, The University of Michigan, Ann Arbor, MI 48109 USA (e-mail: darrens@umich.edu).

C. P. T. Groth is with the Institute for Aerospace Studies, The University of Toronto, North York, Ont., Canada.

K. G. Powell is with the Department of Aerospace Engineering, The University of Michigan, Ann Arbor, MI 48109 USA.

Q. F. Stout is with the Department of Electrical Engineering and Computer Science, The University of Michigan, Ann Arbor, MI 48109 USA.

Publisher Item Identifier S 0093-3813(00)11347-5.

Global computational models based on first principles mathematical descriptions of the physics represent a very important component of efforts to understand space plasma phenomena associated with space weather including the large-scale solar corona, the solar wind, the solar wind interaction with planetary magnetospheres, and the initiation, structure, and evolution of solar wind disturbances. Presently, and in the foreseeable future, numerical models based on the equations of magnetohydrodynamics (MHD) are the only self-consistent mathematical descriptions that can span the enormous distances associated with large-scale space weather phenomena. Although providing only a relatively low-order approximation to the actual behavior of plasmas, MHD models have been used successfully to simulate many important space plasma processes and provide a powerful means for significantly advancing the understanding of such processes.

Global MHD simulations have been used for a long time to simulate the global magnetospheric configuration and to investigate the response of the magnetosphere-ionosphere system to changing solar wind conditions. The first global-scale 3D MHD simulations of the solar wind-magnetosphere system were published in the early 1980s [1]–[4]. Since then, MHD models have been used to study a range of processes. Global MHD models of the magnetosphere are listed in Table I. A recent focus of MHD investigations is the study of magnetospheric “events.” In these simulations, the observed upstream solar wind conditions are used to “drive” the magnetosphere-ionosphere system and numerical predictions are compared with ground based or satellite observations [14]–[16]. In addition to studies of the terrestrial magnetosphere, there have been several applications of MHD models to the study of coronal and solar wind plasma flows. In this paper, however, we limit ourselves to the discussion of global magnetosphere models (even though the issues we raise here also apply to the solar MHD models, as well).

In this paper, we discuss some of the fundamental physical and numerical issues related to constructing modern numerical MHD codes for global, multiscale simulations of space weather in the near-Earth environment. As an example, we apply the model to the interaction of the terrestrial magnetosphere with the solar wind under nominal interplanetary magnetic field (IMF) conditions (when the magnetic field direction is along the nominal Parker spiral).

TABLE I  
GLOBAL MHD MODELS OF THE MAGNETOSPHERE

	Model	Ref.
1	Ogino (1984)	[5]
2	Lyon-Fedder (1986)	[6]
3	Watanabe (1990)	[7]
4	Winglee (1994)	[8]
5	Tanaka (1995)	[9]
6	Raeder (1995)	[10]
7	Janhunen (1996)	[11]
8	ISM (1998)	[12]
9	BATS-R-US (1999)	[13]

## II. BASIC SOLUTION METHODS

The numerical approaches taken in the models listed in Table I vary in a number of details. Models 1, 3, and 4 are based on relatively simple central differencing methods. The Models 2, 5, 6, 7, 8, and 9, however, are based on relatively similar numerical techniques. Models 4, 5, and 7 are based on a high-resolution approach, in which a high-order scheme is blended with a first-order scheme, by means of a nonlinear switch, or limiter [17]. In models 2, 5, 8, and 9, a limited approximation is combined with an approximate Riemann solver. Models 2 and 8 use an approximate Riemann solver based on the five waves associated with the fluid dynamics system, and treats the electromagnetic effects using the constrained-transport technique [18]. Model 6 is similarly structured, but without the use of a Riemann solver; a finite-difference scheme that is conservative for the fluid dynamics system is combined with the constrained-transport technique. Models 5, 7, and 9 use approximate Riemann solvers based on the waves associated with the full magnetohydrodynamic system [19]. Models 2, 5, 6, 8, and 9 are, due to the high-resolution approach, second-order accurate in smooth regions, and locally first-order accurate in discontinuous regions. Model 7 is first-order accurate.

In this paper, we outline the basic elements of a modern, solution adaptive MHD code which is being used for space weather related simulations.

This code (Model 9 in Table I), as explained above, shares many characteristics with other global MHD models. Two features that set it apart are the use of an adaptively refined mesh, and its near-perfect scaling on massively parallel computers. These two features allow the model to be run at dramatically higher resolution than has been achieved to date in global MHD models.

## III. FUNDAMENTALS OF BATS-R-US

### A. Finite-Volume Schemes for Systems of Conservation Laws

A coupled system of conservation laws can be written in the form

$$\frac{\partial \mathbf{U}}{\partial t} + \nabla \cdot \mathbf{F}_{\text{conv}} = \mathbf{S} \quad (1)$$

where  $\mathbf{U}$  is the vector of conserved quantities (e.g., mass,  $x$ -momentum, mass fraction of a particular species, magnetic field, etc.),  $\mathbf{F}_{\text{conv}}$  is the convective flux, and  $\mathbf{S}$  is the source term modeling diffusion, chemical reactions and other effects. We note

that the transport of radiation can also be included in this framework if necessary. Systems of conservation laws lend themselves well to finite-volume discretization. The computational domain is divided into “cells,” typically hexahedra or tetrahedra, and the system of partial differential equations given in (1) is integrated over each cell in the resulting grid. This leads to a set of coupled ordinary differential equations in time, with the cell-averaged values of the conserved quantities as the unknowns. The rate of change of a conserved physical quantity is simply the sum of all fluxes through the faces defining the cell, plus the volume integral of the source terms. This leads to the following ordinary differential equation for the cell volume averaged vector of conserved physical quantities  $\bar{\mathbf{U}}$ :

$$\frac{d\bar{\mathbf{U}}}{dt} = -\frac{1}{\mathcal{V}} \sum_{\text{faces}} \mathbf{F}_{\text{conv}} \cdot \mathbf{A} + \bar{\mathbf{S}} \quad (2)$$

where  $\mathcal{V}$  is the volume of the cell,  $\mathbf{A}$  is the surface area of a given cell face multiplied by the normal vector of the face (the normal vector always points outward of the cell), while  $\bar{\mathbf{S}}$  is the volume average of all source terms. Equation (2) provides an inherently three-dimensional update of  $\bar{\mathbf{U}}$  and it does not separate different directions into different steps (as it is done in operator splitting methods).

The result is a very physical one; each cell in the grid is a small “control volume,” in which the integral form of the conservation laws hold. For example, the time rate of change of the average mass in the cell is expressed in terms of flux of mass through the faces of the cell. In this approach the “quality” of the solution is fundamentally determined by the level of sophistication used in computing the fluxes across cell boundaries.

One distinct advantage of this conservation-law based finite-volume approach is that discontinuous solutions can be achieved, with the proper jump conditions being obeyed, even at the discrete level. For example, any shocks in a flow will satisfy the Rankine–Hugoniot conditions. While this property can be achieved using a scheme derived from a finite-difference approach, it is a natural consequence of adopting a finite-volume point of view.

### B. Weakly Coupled and Strongly Coupled Formulations

Since the governing equations of both magnetohydrodynamics and compressible fluid dynamics can be written in the form given in (1), they can be implemented in a unified framework as long as the left hand side of the equation system is hyperbolic. The hyperbolicity of the system is determined by examining the eigenvalues of the matrices  $\mathbf{M}_x$ ,  $\mathbf{M}_y$ , and  $\mathbf{M}_z$  that arises from rewriting (1) in the quasi-linear form

$$\frac{\partial \mathbf{W}}{\partial t} + \mathbf{M}_x \frac{\partial \mathbf{W}}{\partial x} + \mathbf{M}_y \frac{\partial \mathbf{W}}{\partial y} + \mathbf{M}_z \frac{\partial \mathbf{W}}{\partial z} = \mathbf{S}' \quad (3)$$

where  $\mathbf{W}$  is the vector of primitive variables (such as density, velocity, pressure) and  $\mathbf{S}'$  is the appropriate source term.

If the eigenvalues of  $\mathbf{M}_i$  ( $i = x, y, z$ ) are all real (they need not be distinct, and are typically not in systems of conservation laws), the system is hyperbolic. The eigenvalues and eigenvectors resulting from the decomposition of  $\mathbf{M}_i$  are used to con-

struct the ‘‘Riemann solver’’ that is the heart of modern numerical schemes (Riemann solvers will be discussed later). Both the ideal MHD equations and the equations of compressible fluids are hyperbolic. The coupled system is therefore also hyperbolic, but the eigenvalues and eigenvectors of the coupled system need to be derived to construct the Riemann solver. Thus, the characteristic matrix  $\mathbf{M}_i$  is at the very heart of all numerical schemes, yielding insight into the wave-like character of the coupled equations.

The physical nature of the corresponding eigenvectors (which represent the waves in the system) and eigenvalues (which represent the wave speeds) have a fundamental effect on the quality and robustness of the resulting numerical scheme. This can be demonstrated by considering the following formulation of the equations of ideal MHD (neglecting all external source terms):

$$\frac{\partial \rho}{\partial t} + (\mathbf{u} \cdot \nabla)\rho + \rho(\nabla \cdot \mathbf{u}) = 0 \quad (4)$$

$$\frac{\partial \mathbf{u}}{\partial t} + (\mathbf{u} \cdot \nabla)\mathbf{u} + \frac{1}{\rho}\nabla p = \frac{1}{\mu_0\rho}(\nabla \times \mathbf{B}) \times \mathbf{B} \quad (5)$$

$$\frac{3}{2}\frac{\partial p}{\partial t} + \frac{3}{2}(\mathbf{u} \cdot \nabla)p + \frac{5}{2}p(\nabla \cdot \mathbf{u}) = 0 \quad (6)$$

$$\frac{\partial \mathbf{B}}{\partial t} + (\mathbf{u} \cdot \nabla)\mathbf{B} = (\mathbf{B} \cdot \nabla)\mathbf{u} - \mathbf{B}(\nabla \cdot \mathbf{u}). \quad (7)$$

Here  $\rho$ ,  $\mathbf{u}$ , and  $p$  are the plasma mass density, bulk velocity and total pressure, respectively. In addition,  $\mathbf{B}$  is the magnetic field vector and  $\mu_0$  is the permeability of vacuum. The source term in (5) is the  $\mathbf{j} \times \mathbf{B}$  term, while in (7) we separated the  $\nabla \times (\mathbf{u} \times \mathbf{B})$  term into a convective term for the magnetic field and a source term describing magnetic field distortion.

It can be seen that in (4)–(7) the fluid and electromagnetic equations are coupled through the source terms (no magnetic field effects appear on the left-hand side of the fluid equations). Any corresponding characteristic matrix,  $\mathbf{M}_i$ , has only one nonzero wave speed, the ion-acoustic speed ( $a_s^2 = 5p/3\rho$ ). This formulation of the MHD equations corresponds to *weak electromagnetic coupling*, since the characteristic structure of the equation system is the same as that of the fluid equations alone.

An alternative way of writing (4)–(7) is to move all terms to the left-hand side. This formulation results in a characteristic wave structure which strongly couples electromagnetic and fluid effects and the eigenvalues of matrix  $\mathbf{M}_i$  describe fast and slow magnetosonic and Alfvén waves. This formulation is called *strong electromagnetic coupling*, and, in general, it makes it possible to construct more robust and powerful numerical methods.

The numerical framework used in BATS-R-US is based on the strongly coupled formulation of the full equation system and it is very appropriate for constructing accurate and robust solution methods spanning the vastly different parameter ranges encountered in space environment models.

### C. Symmetrizable Formulation

Modern numerical methods take full advantage of the mathematical structure of the underlying conservation laws. A particular property of some conservation laws which leads

to increased robustness and accuracy is *symmetrizability*. Symmetrizability means that one can find a suitable variable transformation so that the characteristic matrices  $\mathbf{M}_x$ ,  $\mathbf{M}_y$ , and  $\mathbf{M}_z$  all become symmetric. It was shown by Godunov [20] some 25 years ago that symmetrizable systems (and *only* symmetrizable systems) are formally Galilean invariant and that they admit an additional conservation law. Godunov [20] showed that the equations of compressible fluid mechanics are symmetrizable, and the entropy,  $S = p/\rho^\gamma$ , becomes the additional conserved quantity (in addition to the explicit conservation laws for mass, momentum and energy). In this seminal paper, Godunov [20] also showed that in their usual form the equations of magnetohydrodynamics are not symmetrizable, and consequently, they are not mathematically Galilean invariant. In a Galilean invariant system, characteristic wave speeds (with respect to the fluid) are the same in all frames of reference: this is not true for the MHD system in its traditional form.

It was pointed out by Godunov [20] and later by Powell [13] that a more careful formulation of Faraday’s law can be used to avoid the loss of mathematical Galilean invariance. This formulation is based on the recognition that Faraday’s law itself does not specify the value of  $\nabla \cdot \mathbf{B}$ : its value is specified by independent observation (that there are no magnetic monopoles in our Universe). It is shown in advanced textbooks of classical electrodynamics [21], [22] that for an arbitrary vector field the proper form of Faraday’s law is the following (this form is Galilean invariant):

$$\frac{\partial \mathbf{B}}{\partial t} = -\nabla \times \mathbf{E} - (\nabla \cdot \mathbf{B})\mathbf{u}. \quad (8)$$

This equation ensures that the initial value of  $\nabla \cdot \mathbf{B}$  is conserved at all later times. This can be seen by taking the divergence of (8)

$$\frac{\partial(\nabla \cdot \mathbf{B})}{\partial t} + \nabla \cdot [(\nabla \cdot \mathbf{B})\mathbf{u}] = 0. \quad (9)$$

Here the  $\nabla \cdot (\nabla \times \mathbf{E})$  term was dropped since the divergence of a curl is identically zero. Introducing the scalar  $\Psi = (\nabla \cdot \mathbf{B})/\rho$ , (9) can be written as

$$\frac{\partial \rho \Psi}{\partial t} + \nabla \cdot (\rho \mathbf{u} \Psi) = 0. \quad (10)$$

Equation (10) shows that  $\Psi$  is a passively convected scalar which preserves its initial value at all later times (along flow lines). Since at  $t = 0$  the  $\nabla \cdot \mathbf{B} = 0$  initial condition is enforced, the magnetic field vector remains divergenceless everywhere at all later times. This is valid even in closed circulation regions, since in numerical simulations, no portion of the flow is totally cut off from the rest of the flow; even across a theoretically closed streamsurface, numerical dissipation connects the flow on one side to the flow on the other side. In fluid dynamics, there used to be a concern that the vorticity in closed regions of flow simulations was not defined, and could take on arbitrary values. In practice, that did not happen. Similarly, we see that in plasma simulations, even closed streamsurface regions interact with the flow outside them, and there is no accumulation of

$\nabla \cdot \mathbf{B}$  in the rare cases in which closed streamsurfaces occur. Dropping the  $\nabla \cdot \mathbf{B}$  term in (8) over constrains Faraday's law and it results in the loss of formal Galilean invariance.

Using the Galilean invariant form of Faraday's law (8) results in a symmetrizable set of MHD equations. This formulation not only ensures formal Galilean invariance, but it also results in an additional conservation law for the thermodynamic entropy,  $S = p/\rho^\gamma$ . This symmetrizable form is particularly suitable for the unified treatment of MHD and neutral gas equations to be outlined below.

There are alternative methods to handle the solenoidity of the magnetic field. The most widely used ones are the constrained transport method [18] and the projection scheme suggested by Brackbill and Barnes [23]. All these methods have been used with considerable success for magnetospheric simulations.

#### D. High-Resolution Upwind Schemes

Early work in numerical methods for convection-dominated problems showed that results were highly dependent on how the spatial derivatives were numerically calculated. The most straightforward methods, obtained by using symmetric centered differences, led to schemes that were numerically unstable. The most successful schemes were those that used the convection direction to "bias" the numerical representation of the derivatives. These biased schemes are called upwind schemes, because the data used in the update step is biased toward the upwind direction. The simplest upwind scheme for the convection equation

$$\frac{\partial u}{\partial t} + a \frac{\partial u}{\partial x} = 0 \quad (11)$$

is

$$\frac{u_i^{n+1} - u_i^n}{\Delta t} = \begin{cases} -a \frac{u_i^n - u_{i-1}^n}{\Delta x} & a > 0 \\ -a \frac{u_{i+1}^n - u_i^n}{\Delta x} & a < 0 \end{cases} \quad (12)$$

where  $i$  is an index denoting discrete spatial location and  $n$  is an index denoting discrete temporal location.

For systems of conservation laws, use of the upwinding idea relies on:

- doing some type of characteristic decomposition to determine which way is upwind for each of the waves of the system;
- constructing an interface flux based on this characteristic decomposition, using upwind-biased data.

The first step above makes the scheme stable; the second step makes it conservative. There are many ways to carry out the two steps; various approaches lead to a variety of upwind schemes.

Before the development of modern high-resolution upwind schemes, researchers solving hyperbolic systems of conservation laws had a choice between schemes such as Lax–Friedrichs or Rusanov, that were extremely dissipative, or schemes such as Lax–Wendroff, that was much less dissipative but could not capture even weakly discontinuous solutions (e.g., shock waves) without nonphysical and potentially de-stabilizing oscillations in the solutions.

Following the early work of Lax and coworkers [24], [25], Godunov [26], Lax [27], van Leer [28]–[31], [17] Harten [32], Roe [33], Osher [34] and others developed a rich class of schemes for conservation laws. The basic building blocks were:

- Godunov's concept of using the solution to Riemann's initial-value problem as a building-block for a first-order numerical method;
- Van Leer's insight that Godunov's original scheme could be extended to higher order by making the scheme nonlinear;
- Work by Roe, Van Leer, Osher and others on "approximate Riemann solvers," which led to a wide array of schemes that were much less computationally expensive than Godunov's original scheme.

The original Godunov [26] scheme was for a finite-volume scheme for solution of the equations of inviscid, compressible flow of a gas. The seminal idea in this scheme was that, at each time step, the fluxes of mass, momentum and energy through the face connecting two cells of the grid were computed by a solution to Riemann's initial value problem—the early interaction between the fluid states in two neighboring cells were computed numerically from the nonlinear, self-similar problem of the wave interactions between the two fluids. This procedure was carried out for a time  $\Delta t$  at each cell–cell interface in the grid; that constituted one iteration.

This scheme, though computationally expensive and only first-order accurate, turned out to have a huge impact on computational methods for conservation laws. First, the scheme proved to be extremely robust, even for very strong shocks. It was also proven to be much more accurate than the few other schemes that were similarly robust. Also, researchers soon realized that the concept could be carried over to other systems of conservation laws.

Van Leer, who helped popularize Godunov's work in the US, showed that Godunov was unduly pessimistic in his famous theorem that so-called monotonicity-preserving schemes (ones that could capture discontinuous solutions without fear of nonphysical overshoots/undershoots) were inherently limited to first-order accuracy. Van Leer showed that this was true if the scheme was linear, but allowing schemes to depend on the data relieved this constraint, so that schemes that were monotone could also be higher-order. It was this insight that led to schemes like monotone upwind scheme for conservation laws (MUSCL) [29], [17], piecewise-parabolic method (PPM) [35] and essentially nonoscillatory (ENO) [36] in use for conservation laws. All of these methods can be classed as "limited-reconstruction" techniques—interpolation is done to extend the scheme to higher order, but the interpolation is limited in the vicinity of discontinuities, in order to maintain the monotonicity/robustness property.

A number of researchers refined on Godunov's scheme by replacing the exact solution of the Riemann problem with approximate solutions that were cheaper, and had certain nice properties.

One of these "approximate Riemann solvers" that is particularly known due to its high accuracy is Roe's scheme [33]. It will be described briefly here for a one-dimensional system of

conservation laws; its extension to multiple dimensions is relatively straightforward.

Roe's scheme computes the fluxes at a cell interface, based on the states to the left and right of the interface. It does this by looking for simple-wave solutions to the system of conservation laws, and constructing a numerical flux that treats each of these waves in an upwind manner. If the relation

$$\mathbf{U}(x, t) = \mathbf{U}(x - \lambda t) \quad (13)$$

is substituted into the conservation law

$$\frac{\partial \mathbf{U}}{\partial t} + \frac{\partial \mathbf{F}}{\partial x} = 0 \quad (14)$$

the eigenvalue problem

$$\left( \frac{\partial \mathbf{F}}{\partial \mathbf{U}} - \lambda \mathbf{I} \right) \delta \mathbf{U} = 0 \quad (15)$$

results, where  $\mathbf{I}$  is an identity matrix. Roe's scheme is based on the eigenvalues  $\lambda_k$  and right and left eigenvectors  $R_k$  and  $L_k$  that arise from this eigenvalue problem. In general, for a system of  $n$  conservation laws, there will be  $n$  eigenvalues, each with a corresponding left and right eigenvector. The Roe flux is expressed in terms of the states  $\mathbf{U}_L$  and  $\mathbf{U}_R$  just to the left and right of the interface. It can be written as:

- the flux calculated based just on the left state, plus a correction due to waves that are traveling leftwards from the right cell, **or**
- the flux calculated based just on the right state, plus a correction due to waves that are traveling rightwards from the left cell, **or**
- a symmetric form that arises from averaging the above two expressions. This last is given by

$$\mathbf{F}_{\text{interface}} = \frac{1}{2} [\mathbf{F}(\mathbf{U}_L) + \mathbf{F}(\mathbf{U}_R)] - \frac{1}{2} \sum_{k=1}^n R_k |\lambda_k| L_k (\mathbf{U}_R - \mathbf{U}_L). \quad (16)$$

Research into approximate Riemann solvers led to robust and low dissipation schemes for gasdynamics, like Roe's scheme [33], Osher's scheme [34], [37], and their extension to other systems of conservation laws (such as magnetohydrodynamics). These algorithmic advances yielded methods that had the minimum dissipation necessary to provide stability—they provided robustness nearly equal to that of the Lax–Friedrichs scheme in conjunction with accuracy near that of the Lax–Wendroff scheme. These schemes, when coupled with the limited-reconstruction techniques described above, provided the accurate, robust, efficient schemes that can generally be classed as high-resolution methods.

Our approach takes advantage of these advances in approximate Riemann solvers and limited reconstruction. The limited reconstruction approach ensures second-order accuracy away from discontinuities, while simultaneously providing the stability that ensures nonoscillatory solutions. Modern limiters will

be used, to ensure these properties. The approximate Riemann solver approach ensures correct capturing of discontinuous solutions, and a robustness across a wide range of flow parameters.

Diffusive fluxes can be handled with a Galerkin-based approach, to ensure accurate discretization of those terms. Source terms are handled point-implicitly to help alleviate stiffness due to differences in time scales between reactive and convective processes.

### E. Building “Smart” Codes through Use of Solution Adaptation

A solution-adaptive grid is a virtual necessity for resolving a problem with disparate length scales. In order to avoid under-resolving high-gradient regions in the problem, or, conversely, over-resolving low-gradient regions at the expense of more critical regions, solution adaptation is a powerful tool, saving several orders of magnitude in computing resources for many problems. Length scales in spaceweather simulations range from a few kilometers to  $10^8$  km; time scales range from a few seconds to  $10^5$  s. These problems cry out for solution-adaptive schemes—a simple nonadapted mesh would grossly underresolve much of the problem, while overresolving relatively uninteresting regions. To demonstrate this point we mention that to resolve the sun–earth distance with a uniform resolution of 10 km in three dimensions would require about  $10^{24}$  computational cells. To carry out such a simulation is clearly beyond anyone's computational capabilities for a long time to come.

Typical calculations have 10–15 levels of refinement; some calculations have more than 20 levels of refinement. In the case of 20 levels of refinement, the finest cells on the mesh are more than one million times smaller in each dimension than the coarsest cells on a mesh.

### F. Harnessing the Power of Massively Parallel Computers

Massively parallel machines entice users with a factor of 512, or 1024, or even more in CPU and memory resources than single-processor machines. Capitalizing on the promise of these resources is, however, not always straightforward. In general, researchers have had very poor luck with “automatically parallelizing” their codes, or, more generally, with porting legacy codes to this class of machines. For most codes based on solving PDEs that model physical processes, *domain decomposition*, i.e., partitioning the problem by dividing the computational domain into sections, and farming the separate sections off onto separate processors, is the most practical approach. However, codes that were designed with single-processor computing in mind, may have inherent limits as to their scalability, and may, for example, achieve a speed-up for 16, or 32, or 64 processors, with added processors not only failing to speed the code up further, but actually slowing down the code. These inherent limitations can arise from a variety of sources:

- underlying basic algorithms that are global in nature, resulting in high communication costs;
- underlying data structures that are expensive to partition or to update in a parallel fashion;
- underlying processes that are inherently serial.

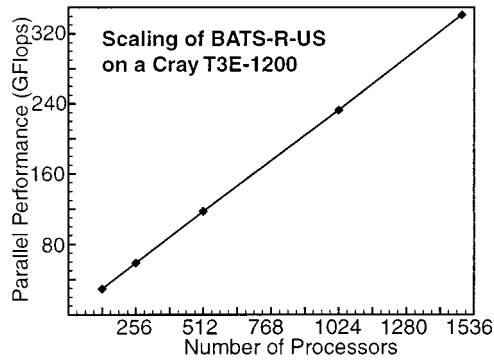


Fig. 1. Parallel performance (on a linear scale) of BATS-R-US on a Cray-T3E-1200 supercomputer.

In order to avoid any of these limitations, the approach taken in BATS-R-US is designed with parallelism in mind. The underlying basic algorithm is highly local in nature, resulting in low communication overhead. The data structures on which the code is built allow easy, natural partitioning of the data, and greatly facilitate load-balancing, a crucial element of truly scalable computing. The design was carried out in such a way that even the adaptation of the grid could be carried out in parallel. A detailed description of the code is given by Powell *et al.* [13], and by Groth *et al.* [38], [39]. The application of BATS-R-US to space weather research is discussed in a companion paper [40].

The performance of the code on a massively parallel machine is shown in Fig. 1. As can be seen from the plot, the code scales nearly perfectly; that is, doubling the number of processors allows one to run on twice as fine a mesh in the same amount of time.

The underlying numerical scheme of the model has been validated on some general benchmark problems [13], and the full adaptive parallel code has been validated on a number of space-physics problems by comparison to observation [41]–[45] and by a grid-convergence study [46].

#### IV. APPLICATION TO THE MAGNETOSPHERE

The BATS-R-US code has been successfully applied to the simulation of a broad range of space plasmas ranging from solar coronal expansion [47], [39], [48], to the interaction of the heliosphere with the interstellar medium [49], to the magnetospheres of Mercury [50], [51], Venus [43], Earth [52], [53], [45], Mars [54], and Saturn [55], [50]. In addition, we successfully simulated the interaction of comets with the solar wind [41], [56] including the emission of cometary x-rays [42], the interaction of Io [44], Europa [57], and Titan [58] with the high speed magnetospheric plasma. Here we present an example describing the interaction of the solar wind with the terrestrial magnetosphere when the IMF is along the nominal (Parker spiral) direction [53].

##### A. Intrinsic Magnetic Field

The simulation of the interaction between the solar wind and a strongly magnetized planet represents several computational challenges. One of the difficulties arises from the large dynamic range of the magnetic field. The typical magnitude of the interplanetary magnetic field (IMF) is about 10 nT, while the mag-

netic field magnitude near the magnetic pole of Earth (at  $1 R_E$ ) is about  $6 \times 10^4$  nT. The magnetic terms (stress and energy) in (5) are quadratic, therefore the dynamic range of magnetic field effects can reach eight orders of magnitude. In addition, the intrinsic magnetic field is not far from a dipole field, therefore the radial dependence of the magnetic terms in the momentum and energy equations is very steep in the near Earth region ( $|\nabla B^2| \sim r^{-7}$ ). It is very difficult to resolve such steep gradients in 3-D numerical simulations.

The difficulty of the numerical solution can be significantly reduced by separating the magnetic field into an “intrinsic” and a “deviative” component as suggested by [9]. It should be emphasized that the deviative component does not have to be small: we simply separate the contribution of the known intrinsic magnetic field from the total field. The method does not neglect any of the terms describing the nonlinear interaction between the intrinsic and deviative magnetic fields: it only analytically assures cancellations of large terms (which numerically may not cancel exactly due to the finite accuracy of computers). The advantage of this method is that the high spatial gradients of the known terrestrial magnetic field can be treated analytically at the differential equation level.

##### B. Ionosphere-Magnetosphere Coupling

Coupling between the magnetosphere and ionosphere is accounted for by using a height-integrated electrostatic model of the ionosphere, in which closure of the field-aligned current system arising from the MHD solution is modeled at the ionospheric boundary by applying the principle of current conservation. In particular, Ohm’s law is applied to a thin spherical shell [59], [60]. An elliptic equation for the ionospheric electric potential on the spherical shell involving height-integrated conductivities (conductances) is solved and the resulting potential solution is used to prescribe the plasma convection velocity at the ionospheric boundary (i.e., the ionospheric potential solution provides boundary conditions for plasma velocity of the MHD solution at the magnetosphere-ionosphere interface). The field-aligned current from the magnetosphere solution and the resulting electric field from the ionosphere solution are mapped along the dipole field lines between the inner boundary of the magnetosphere and the ionospheric surface, thereby providing coupling between the magnetosphere and ionosphere.

##### C. Boundary Conditions

Boundary conditions are enforced with the help of “ghost cells” which are either cells just outside the simulation box, or just inside the magnetosphere-ionosphere boundary. Our boundary procedure prescribes the values of physical quantities in the ghost cells, and the approximate Riemann-solver self-consistently calculates the fluxes across the interface. This method not only provides a physical way to implement boundary conditions, but is also numerically robust and capable of correcting some inconsistencies (the fluxes carry only the physically necessary information from the ghost cell into the simulation domain).

At the upstream boundary a free streaming solar wind enters the computational domain. At the other five outer boundaries the

ghost cells contain free-streaming solar wind conditions. Since these boundaries are far enough away so that the plasma flow is supersonic and superalfvénic at these locations, the physical parameters in the ghost cells are greatly flexible, as long as all eight characteristics point outward of the simulation domain. Our boundary conditions ensure this property.

The inner boundary of the simulation was at  $3 R_E$ . At the inner boundary the boundary conditions described no mass flux across the boundary. Reflective boundary conditions were used for the mass density and kinetic pressure. Neumann conditions were applied for the tangential components of the deviative magnetic field (the difference between the dipole magnetic field and the actual field) and Dirichlet condition for the normal component.

#### D. Results for Parker Spiral IMF Conditions

The input parameters used in the present simulation are based on the GGCM Phase-1 parameter suite and they differ only in the IMF direction. The GGCM Phase-1 steady-state simulation suite input parameters describe a steady solar wind flow along the sun–earth line, a nontilted terrestrial magnetic dipole located at the center of the Earth, and a uniform, constant conductance tensor in the ionosphere ( $\Sigma_P = 5 \text{ S}$ ,  $\Sigma_H = 0$ , and  $\Sigma_0 \gg 1$ ). The IMF magnitude was chosen to be  $B = 10 \text{ nT}$ , which is one of the GGCM Phase-1 cases (the other value is  $5 \text{ nT}$ ). The IMF direction was assumed to be along the nominal Parker-spiral, therefore the IMF vector is given by  $\mathbf{B} = (-\sqrt{50}, \sqrt{50}, 0) \text{ nT}$  (the  $x$  axis points toward the Sun, the  $z$  axis points to north and  $y$  axis makes the coordinate system right handed).

The computational domain extends from  $x = 192 R_E$  to  $x = -384 R_E$  along the sun–earth direction and from  $-192 R_E$  to  $192 R_E$  in the  $y$  and  $z$  directions. The smallest cells are  $1/4 R_E$  near the inner boundary, while the largest cells are  $32 R_E$ . We used 7 levels of refinement in the simulation. The large distance between the upstream boundary and Earth was chosen to ensure that all boundaries are far from the physically most interesting regions.

The inner boundary of the simulation is at  $3 R_E$ . The MHD simulation domain is connected to the height integrated ionosphere (located at  $1 R_E$ ) by unperturbed dipole field lines. Field aligned currents (FACs) are mapped along undisturbed dipole field lines between the MHD magnetosphere and electrostatic ionosphere. This procedure is described in detail by Goodman [59]. Plasma flow is not allowed through the inner boundary, and the field aligned current is allowed to freely penetrate into the electrostatic ionosphere.

1) *Last Closed Field Lines*: Our simulation uses quite similar conditions to those used in the recently published simulation of White *et al.* [12]. The main difference is that [12] considered a pure  $B_y = 5 \text{ nT}$  IMF, while our simulation also includes a  $B_x$  component ( $B_x = -B_y$ ) and uses a stronger total magnetic field. The reason for the inclusion of a  $B_x$  component is that this IMF direction is closer to the observed average conditions and therefore comparison with observed magnetospheric topologies is somewhat easier. In spite of the difference in input parameters the simulated magnetospheric configuration and topology are quite similar to those reported by White *et al.* [12], including the formation of the magnetospheric sash.

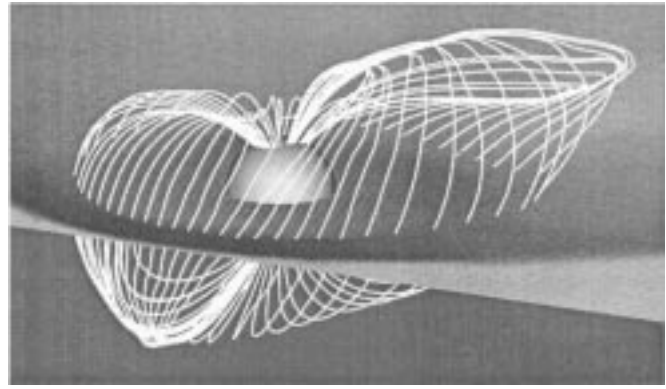


Fig. 2. Three-dimensional representation of the last closed field lines. Also shown is the equatorial plane with the computational grid. The grayscale represents the normalized thermal pressure of the plasma.

Fig. 2 shows a three-dimensional rendering of the last closed field lines (on the dayside this is essentially the magnetopause). The figure also shows the equatorial plane with the computational grid. The grayscale represents the normalized thermal pressure of the plasma. One of the most interesting features of the magnetopause is the counterclockwise twist of the symmetry plane from  $z = 0$ . This twist is a consequence of the positive IMF  $B_y$  component [61].

It is interesting to note that for IMF  $B_z = 0$  the magnetospheric topology is very similar to the southward IMF configuration. Magnetic reconnection takes place along the “sash” as described by White *et al.* [12]. The reconnected field lines move downstream and form the open magnetic topology of the magnetotail. A near-earth neutral line is formed at around  $17 R_E$  downstream behind earth. At this line the reconnected IMF field lines “disconnect” from the geomagnetic field lines and form highly draped IMF field lines. These field lines play an important role in determining the topology of the magnetotail.

2) *Magnetotail Topology*: The left panel in Fig. 3 shows simulated two-dimensional “magnetic streamlines” in a cross-sectional plane in the magnetotail. These magnetic streamlines are generated by drawing the two-dimensional field lines defined by the  $B_y$  and  $B_z$  components of the three-dimensional magnetic field vector. Real three-dimensional magnetic field lines come out of (and go into) the plane, due to the (generally) nonzero  $B_x$  component. Thus, the magnetic streamline topology in tail cross sections does not fully characterize the magnetic structure of the tail. The advantage of using these streamlines is that they are relatively easy to visualize and there is a new body of observational evidence which can be compared with the simulation results [62].

The left panel in Fig. 3 shows simulated magnetic streamlines in a tail cross section (located around the middle of the closed magnetotail), while the right panel is the magnetic streamline pattern synthesized from four years of IMP 8 observations for IMF  $B_y > 0$  conditions [62].

Cross-sectional patterns like those in Fig. 3 are typically characterized by the critical points [63], i.e., points at which  $B_y = B_z = 0$ . These critical points can be classified as stable or unstable nodes, saddles, centers, or stable or unstable spirals; the classification depends on local values of  $\partial B_y / \partial y$  and  $\partial B_z / \partial z$ . While it is easy to misinterpret these critical points, since the

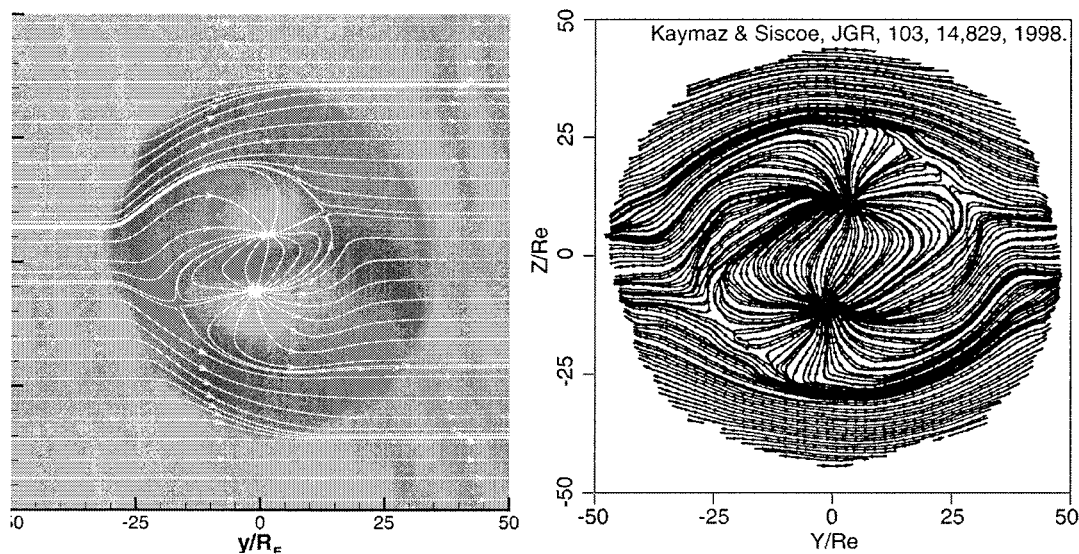


Fig. 3. Magnetic streamlines in a cross-sectional plane of the magnetotail for IMF  $B_y > 0$  conditions. The left panel is from the present simulation (the background grayscale characterizes the logarithm of the normalized pressure), while the right panel is a synthesis of four years of IMP 8 observations [62].

$B_x$  component is ignored, they do correspond to certain physical situations. For example, a node corresponds to the magnetic field lines turning from a three-dimensional orientation to one parallel to the sun–earth axis.

The similarity between the simulated (left panel of Fig. 3) and observed (right panel of Fig. 3) magnetic streamlines is striking. The two patterns are topologically identical, with both exhibiting two saddles and two nodes: a stable node in the upper half plane (the magnetic streamlines converge on the node) and an unstable node in the lower half plane (the magnetic streamlines leave the node). Even the location and orientation of these critical points is quite similar. The radius of the simulated magnetotail is smaller than the observations indicate, due to the stronger than average IMF magnitude (10 nT) used in the simulation. However, this small difference does not effect the excellent agreement between the simulated and observed magnetotail topologies.

There are three types of magnetic streamlines in Fig. 3: fully open, reconnected and closed. Fully open streamlines pass completely through the plot without connecting to a node or a saddle. These streamlines correspond to interplanetary magnetic field lines. Some of these streamlines pass through the bow shock and exhibit a kink, some of them are located above or below the shock and they pass through the Figure without any distortion. Reconnected interplanetary magnetic field lines either enter the figure from the left and connect to the stable node on the north, or originate from the unstable node on the south and leave the figure to the right. These streamlines correspond to interplanetary magnetic field lines which reconnect to the geomagnetic field in the northern (stable node) or southern (unstable node) cusp. Finally, closed magnetic streamlines originate from the southern (unstable) node and go into the northern (stable) node. These correspond to closed geomagnetic field lines.

The three-dimensional magnetotail topology corresponding to the streamline topology shown in Fig. 3 describes an open magnetotail as discussed by Kaymaz and Siscoe [62]. The separatrix between reconnected and closed field lines corresponds

to the magnetopause. The two saddle points correspond to the magnetospheric sash [12] characterized by low magnetic field magnitudes. The nodes correspond to sun–earth aligned magnetic field lines connecting to the cusps.

## REFERENCES

- [1] J. N. LeBoeuf, T. Tajima, C. F. Kennel, and J. M. Dawson, "Global simulations of the three-dimensional magnetosphere," *Geophys. Res. Lett.*, vol. 8, p. 257, 1981.
- [2] C. C. Wu, R. J. Walker, and J. M. Dawson, "A three-dimensional MHD model of the Earth's magnetosphere," *Geophys. Res. Lett.*, vol. 8, p. 523, 1981.
- [3] S. H. Brecht, J. Lyon, J. A. Fedder, and K. Hain, "A simulation study of east-west IMF effects on the magnetosphere," *Geophys. Res. Lett.*, vol. 8, p. 397, 1981.
- [4] —, "A time-dependent three-dimensional simulation of the earth's magnetosphere: Reconnection events," *J. Geophys. Res.*, vol. 87, p. 6098, 1982.
- [5] T. Ogino and R. J. Walker, "A magnetohydrodynamic simulation of the bifurcation and tail lobes during intervals with a northward interplanetary magnetic field," *Geophys. Res. Lett.*, vol. 11, p. 1018, 1984.
- [6] J. G. Lyon, J. A. Fedder, and J. G. Huba, "The effect of different resistivity models on magnetotail dynamics," *J. Geophys. Res.*, vol. 91, p. 8057, 1986.
- [7] K. Watanabe and T. Sato, "Global simulation of the solar wind-magnetosphere interaction: The importance of its numerical validity," *J. Geophys. Res.*, vol. 95, p. 75, 1990.
- [8] R. M. Winglee, "Non-MHD influences on the magnetospheric current system," *J. Geophys. Res.*, vol. 99, p. 13,437, 1994.
- [9] T. Tanaka, "Generation mechanisms for magnetosphere-ionosphere current systems deduced from a three-dimensional MHD simulation of the solar wind-magnetosphere-ionosphere coupling process," *J. Geophys. Res.*, vol. 100, p. 12,057, 1995.
- [10] J. Raeder, R. J. Walker, and M. Ashour-Abdalla, "The structure of the distant geomagnetic tail during long periods of northward IMF," *Geophys. Res. Lett.*, vol. 22, p. 349, 1995.
- [11] P. Janhunen, "GUMICS-3: A global ionosphere-magnetosphere coupling simulation with high ionospheric resolution," in *Proc. ESA 1996 Symposium on Environment Modeling for Space-Based Applications*, 1996, ESA SP-392, pp. 233–239.
- [12] W. W. White, G. L. Siscoe, G. M. Erickson, Z. Kaymaz, N. C. Maynard, K. D. Siebert, B. U. Ö. Sonnerup, and D. R. Weimer, "The magnetospheric sash and the cross-tail S," *Geophys. Res. Lett.*, vol. 25, p. 1605, 1998.

- [13] K. G. Powell, P. L. Roe, T. J. Linde, T. I. Gombosi, and D. L. DeZeeuw, "A solution-adaptive upwind scheme for ideal magnetohydrodynamics," *J. Comput. Phys.*, vol. 154, p. 284, 1999.
- [14] J. A. Fedder, S. P. Slinker, J. G. Lyon, and R. D. Elphinstone, "Global numerical simulation of the growth phase and the expansion onset for a substorm observed by Viking," *J. Geophys. Res.*, vol. 100, p. 19083, 1995.
- [15] J. A. Fedder, S. P. Slinker, and J. G. Lyon, "A comparison of global numerical simulation results to data for the January 27–28, 1992, Geospace Environment Modeling challenge eventpo," *J. Geophys. Res.*, vol. 103, p. 14799, 1998.
- [16] J. Raeder, J. Berchem, and M. Ashour-Abdalla, "The geospace environment modeling grand challenge: Results from a global geospace circulation model," *J. Geophys. Res.*, vol. 103, p. 14787, 1998.
- [17] B. van Leer, "Toward the ultimate conservative difference scheme. V. A second-order sequel to Godunov's method," *J. Comput. Phys.*, vol. 32, p. 101, 1979.
- [18] C. R. Evans and J. F. Hawley, "Simulation of magnetohydrodynamic flows: A constrained transport method," *Astrophysical Journal*, vol. 332, p. 6597, 1988.
- [19] K. G. Powell, "An approximate Riemann solver for magnetohydrodynamics (that works in more than one dimension)," Tech. Rep. 94-24, ICASE, Langley, VA, 1994.
- [20] S. K. Godunov, "Symmetric form of the equations of magnetohydrodynamics" (in Russian), in *Numerical Methods for Mechanics of Continuum Medium*: Siberian Branch of USSR Academy of Sciences, 1972, vol. 1, pp. 26–34.
- [21] W. K. H. Panofsky and M. Phillips, *Classical Electricity and Magnetism*. Reading, MA: Addison Wesley, 1955.
- [22] J. D. Jackson, *Classical Electrodynamics*. New York: Wiley, 1975.
- [23] J. U. Brackbill and D. C. Barnes, "The effect of nonzero  $\nabla \cdot \mathbf{B}$  on the numerical solution of the magnetohydrodynamic equations," *J. Comput. Phys.*, vol. 35, p. 426, 1980.
- [24] P. D. Lax, "Weak solution of nonlinear hyperbolic equations and their numerical computation," *Communications on Pure and Applied Mathematics*, vol. 7, pp. 159–193, 1954.
- [25] P. D. Lax and B. Wendroff, "Systems of conservation laws," *Communications on Pure and Applied Mathematics*, vol. 13, p. 217, 1960.
- [26] S. K. Godunov, "A difference scheme for numerical computation of discontinuous solutions of hydrodynamic equations" (in Russian), *Mat. Sb.*, vol. 47, p. 271, 1959.
- [27] P. D. Lax, "Hyperbolic systems of conservation laws and the mathematical theory of shock waves," in *CMBS-NSF Regional Conference Series in Applied Mathematics*. Philadelphia: Society for Industrial and Applied Mathematics, 1973, vol. 11.
- [28] B. van Leer, "Toward the ultimate conservative difference scheme. I. The quest of monotonicity," *Lecture Notes in Physics*, vol. 18, p. 163, 1973.
- [29] —, "Toward the ultimate conservative difference scheme. II. Monotonicity and conservation combined in a second-order scheme," *J. Comput. Phys.*, vol. 14, p. 361, 1974.
- [30] —, "Toward the ultimate conservative difference scheme. III. Upstream-centered finite-difference schemes for ideal compressible flow," *J. Comput. Phys.*, vol. 23, p. 263, 1977.
- [31] —, "Toward the ultimate conservative difference scheme. IV. A new approach to numerical convection," *J. Comput. Phys.*, vol. 23, p. 276, 1977.
- [32] A. Harten, "The artificial compression method for computation of shocks and contact discontinuities: III. Self-adjusting hybrid schemes," *Math. Comput.*, vol. 32, p. 363, 1976.
- [33] P. L. Roe, "Approximate Riemann solvers, parameter vectors, and difference schemes," *J. Comput. Phys.*, vol. 43, p. 357, 1981.
- [34] S. Osher, "Riemann solvers, the entropy condition, and difference approximations," *SIAM J. Numer. Anal.*, vol. 21, p. 217, 1984.
- [35] P. Woodward and P. Colella, "The piecewise parabolic method for gas dynamical calculations," *J. Comput. Phys.*, vol. 32, p. 101, 1979.
- [36] S. K. Chakravarthy, A. Harten, and S. Osher, "Essentially nonoscillatory shock-capturing schemes of arbitrarily-high accuracy," Paper 86-0339, AIAA, 1986.
- [37] A. Harten, P. D. Lax, and B. van Leer, "On upstream differencing and Godunov-type schemes for hyperbolic conservation laws," *SIAM Rev.*, vol. 25, p. 35, 1983.
- [38] C. P. T. Groth, D. L. De Zeeuw, K. G. Powell, T. I. Gombosi, and Q. F. Stout, "A parallel solution-adaptive scheme for ideal magnetohydrodynamics," in *Proc. AIAA 14th Computational Fluid Dynamics Conference*, June 1999, Paper no. 99-3273.
- [39] C. P. T. Groth, D. L. De Zeeuw, T. I. Gombosi, and K. G. Powell, "Global 3D MHD simulation of a space weather event: CME formation, interplanetary propagation, and interaction with the magnetosphere," *J. Geophys. Res.*, 2000, to be published.
- [40] C. R. Clauer, T. I. Gombosi, D. L. De Zeeuw, A. J. Ridley, K. G. Powell, B. van Leer, Q. F. Stout, C. P. T. Groth, T. E. Holzer, and R. A. Wolf, "High-performance computer methods applied to predictive space weather simulations," *IEEE Trans. Plasma Sci.*, 2000.
- [41] T. I. Gombosi, D. L. De Zeeuw, R. M. Häberli, and K. G. Powell, "Three-dimensional multiscale MHD model of cometary plasma environments," *J. Geophys. Res.*, vol. 101, p. 15233, 1996.
- [42] R. M. Häberli, T. I. Gombosi, D. L. DeZeeuw, M. R. Combi, and K. G. Powell, "Modeling of cometary x-rays caused by solar wind minor ions," *Science*, vol. 276, p. 939, 1997.
- [43] R. Bauske, A. F. Nagy, T. I. Gombosi, D. L. De Zeeuw, K. G. Powell, and J. G. Luhmann, "A three-dimensional MHD study of solar wind mass loading processes at Venus: Effects of photoionization, electron impact ionization, and charge exchange," *J. Geophys. Res.*, vol. 103, p. 23625, 1998.
- [44] M. R. Combi, K. Kabin, T. I. Gombosi, D. L. De Zeeuw, and K. G. Powell, "Io's plasma environment during the Galileo flyby: Global three-dimensional MHD modeling with adaptive mesh refinement," *J. Geophys. Res.*, vol. 103, p. 9071, 1998.
- [45] P. Song, D. L. De Zeeuw, T. I. Gombosi, C. P. T. Groth, and K. G. Powell, "A numerical study of solar wind—Magnetosphere interaction for northward IMF," *J. Geophys. Res.*, vol. 104, p. 28361, 1999.
- [46] T. I. Gombosi, K. G. Powell, and B. van Leer, "Comment on "Modeling the magnetosphere for northward interplanetary magnetic field: Effects of electrical resistivity" by Joachim Raeder," *J. Geophys. Res.*, vol. 105, 2000, to be published.
- [47] C. P. T. Groth, D. L. De Zeeuw, T. I. Gombosi, and K. G. Powell, "Three-dimensional MHD simulation of coronal mass ejections," *Adv. Space Res.*, 1998, to be published.
- [48] T. I. Gombosi, D. L. De Zeeuw, C. P. T. Groth, K. G. Powell, and Q. F. Stout, "Multiscale MHD simulation of a coronal mass ejection and its interaction with the magnetosphere-ionosphere system," *J. Atmos. Solar-Terr. Phys.*, 2000, to be published.
- [49] T. J. Linde, T. I. Gombosi, P. L. Roe, K. G. Powell, and D. L. De Zeeuw, "The heliosphere in the magnetized local interstellar medium: Results of a 3D MHD simulation," *J. Geophys. Res.*, vol. 103, p. 1889, 1998.
- [50] T. I. Gombosi, D. L. De Zeeuw, C. P. T. Groth, K. C. Hansen, K. Kabin, and K. G. Powell, "MHD simulations of current systems in planetary magnetospheres: Mercury and Saturn," in *Magnetospheric Current Systems*, R. Fujii, M. Hesse, R. Lysak, and S. Ohtani, Eds., Aug. 1999, to be published.
- [51] K. Kabin, T. I. Gombosi, D. L. De Zeeuw, and K. G. Powell, "Interaction of mercury with the solar wind," *Icarus*, vol. 143, p. 397, 2000.
- [52] T. I. Gombosi, D. L. De Zeeuw, C. P. T. Groth, K. G. Powell, and P. Song, "The length of the magnetotail for northward IMF: Results of 3D MHD simulations," in *Phys. Space Plasmas (1998)*, vol. 15, T. Chang and J. R. Jasperse, Eds, 1998, pp. 121–128.
- [53] T. I. Gombosi, D. L. De Zeeuw, C. P. T. Groth, and K. G. Powell, "Magnetospheric configuration for parker-spiral IMF conditions: Results of a 3D AMR MHD simulation," *Adv. Space Res.*, vol. 21, no. 1, p. 139, 2000.
- [54] Y. Liu, A. F. Nagy, C. P. T. Groth, D. L. De Zeeuw, T. I. Gombosi, and K. G. Powell, "3D multi-fluid MHD studies of the solar wind interaction with Mars," *Geophys. Res. Lett.*, vol. 26, p. 2689, 1999.
- [55] K. C. Hansen, T. I. Gombosi, D. L. DeZeeuw, C. P. T. Groth, and K. G. Powell, "A 3D global MHD simulation of Saturn's magnetosphere," *Adv. Space Res.*, 1999, to be published.
- [56] P. L. Israelevich, T. I. Gombosi, A. I. Ershkovich, D. L. DeZeeuw, F. M. Neubauer, and K. G. Powell, "The induced magnetosphere of comet Halley, 4: Comparison of in situ observations and numerical simulations," *J. Geophys. Res.*, vol. 104, p. 28309, 1999.
- [57] K. Kabin, M. R. Combi, T. I. Gombosi, A. F. Nagy, D. L. De Zeeuw, and K. G. Powell, "On Europa's magnetospheric interaction: An MHD simulation of the E4 flyby," *J. Geophys. Res.*, vol. 104, p. 19983, 1999.
- [58] K. Kabin, T. I. Gombosi, D. L. DeZeeuw, K. G. Powell, and P. L. Israelevich, "Interaction of the Saturnian magnetosphere with Titan: Results of a 3D MHD simulation," *J. Geophys. Res.*, vol. 104, p. 2451, 1999.

- [59] M. L. Goodman, "A three-dimensional iterative, mapping procedure for the implementation of an ionosphere-magnetosphere anisotropic Ohm's law boundary condition in global magnetohydrodynamic simulations," *Annales Geophysicae*, vol. 13, p. 843, 1995.
- [60] O. Amm, "Comment on 'A three-dimensional, iterative, mapping procedure for the implementation of an ionosphere-magnetosphere anisotropic Ohm's law boundary condition in global magnetohydrodynamic simulations' by Michael L. Goodman," *Annales Geophysicae*, vol. 14, p. 773, 1996.
- [61] Z. Kaymaz, G. L. Siscoe, J. G. Luhmann, R. P. Lepping, and C. T. Russell, "Interplanetary magnetic field control of magnetotail magnetic geometry: IMP 8 observations," *J. Geophys. Res.*, vol. 99, p. 11 113, 1994.
- [62] Z. Kaymaz and G. L. Siscoe, "Open geometry of the magnetotail cross section," *J. Geophys. Res.*, vol. 103, p. 14 829, 1998.
- [63] J. H. B. Smith, "Remarks on the structure of conical flow," *Progress in Aerospace Sciences*, vol. 12, p. 241, 1972.

**Darren L. De Zeeuw** received the Ph.D. degree in aerospace engineering and scientific computing from the University of Michigan in 1993.

As a graduate student he developed an algorithm which solved the two dimensional Euler equations using a quadtree-based unstructured Cartesian grid with adaptive refinement and multigrid convergence acceleration. Upon completion of his dissertation work, Dr. De Zeeuw joined the Space Physics Research Laboratory to work with the space plasma simulation group to develop a magnetohydrodynamic (MHD) model based on his dissertation work. This model has been developed to a fully three dimensional high-performance MHD model which incorporates a new Roe-type MHD Riemann solver. This model includes adaptive refinement, allowing it to give enhanced resolution in regions of interest. The code achieved a sustained performance of 345 GFlops on a Cray T3E-1200 supercomputer with 1490 PEs.

**Tamas I. Gombosi** was educated in theoretical physics at the Lóránd Eötvös University in Budapest, Hungary. He did his post-doctoral research at the Space Research Institute in Moscow under the direction of Dr. Konstantin Gringauz.

In 1987, he joined the University of Michigan where he is presently Professor of Space Science and Professor of Aerospace Engineering. Prof. Gombosi's research interests span from the physics of comets, through heliospheric plasmas to planetary plasma environments. He served as Editor-in-Chief of the *Journal of Geophysical Research-Space Physics* (1992–1997). He also served on a large number of national and international scientific committees, including the Committee on Solar and Space Physics of the Space Studies Board (National Academy of Sciences), and is presently Chairman of Commission D (Space Plasmas) of COSPAR.

Prof. Gombosi is recipient of several scientific awards. He is an elected Member of the International Academy of Astronautics, and a Fellow of the American Geophysical Union. Prof. Gombosi is author or co-author of over 150 refereed publications and gave over 200 scientific presentations. He published two graduate level textbooks: "Gaskinetic Theory" (Cambridge, 1994) and "Physics of the Space Environment" (Cambridge, 1998).

**Clinton P. T. Groth** received the Ph.D. degree in aerospace science and engineering from the University of Toronto in 1993. His doctoral dissertation was concerned with the use of high-resolution finite-volume schemes for the numerical solution of partial-differential equations governing thermochemical nonequilibrium flows with strong shocks.

Prof. Groth was the 1991 recipient of the G. N. Patterson Award and a 1992–1993 University of Toronto Governor General's Gold Medal. In 1993 Prof. Groth joined the University of Michigan as a post-doctoral research fellow. There he studied generalized transport theory and the use of higher-order moment closures for the solution of the Boltzmann equation in conjunction with advanced numerical methods. This research led to a new hierarchy of moment closures with several desirable mathematical features that appears to offer improved modeling of transition-regime flows of rarefied gaseous and anisotropic space plasmas. Subsequently, Prof. Groth joined the Space Physics Research Laboratory at the University of Michigan in 1995 as an Assistant Research Scientist and in 1999 joined the faculty of the University of Toronto as an Assistant Professor. Prof. Groth has authored or co-authored seven journal articles, and nine refereed papers in conference proceedings. He is a member of the American Institute of Aeronautics and Astronautics, American Geophysical Union, Society for Industrial and Applied Mathematics, and Canadian Aeronautics and Space Institute.

**Kenneth G. Powell** received the doctorate degree in aeronautics and astronautics from MIT in 1987, where Dr. Earl Murman was his thesis advisor. His doctoral work was in the computational modeling of vortical flows; his thesis was published as a research monograph in the series "Notes on Numerical Fluid Mechanics."

He was a recipient of a NASA Group Achievement Award in 1989 for his work in vortical flows. After leaving MIT, he joined the faculty in the Aerospace department at the University of Michigan. Prof. Powell has branched out into the research areas of solution-adaptive schemes, genuinely multidimensional schemes for compressible flows, and, most recently, numerical methods for magnetohydrodynamics. He was a National Science Foundation Presidential Young Investigator from 1988–1994.

**Quentin F. Stout** received the Ph.D. degree in mathematics.

For over 15 years, he has worked in the areas of parallel computing and parallel algorithms. His emphasis has been on developing parallel algorithms and data structures that are as scalable as possible, on developing parallel programming paradigms, and on developing systematic techniques for improving parallel efficiency. He also analyzed limits to parallel performance, from both theoretical viewpoints and from experimental viewpoints based on the hardware/software characteristics of specific systems. His professional activities in parallel computing include co-authoring the book *Parallel Algorithms for Regular Architectures: Meshes and Pyramids* (Cambridge: Mass. Inst. Technol. Press, 1996); writing over 100 articles and book chapters; editing three parallel computing journals and a book on reconfigurable architectures; co-chairing the program for three international conferences (and being on the program committee of many others); lecturing at NATO Advanced Study Institutes; and giving tutorials on parallel computing at numerous conferences, corporations, and government agencies. He is the Director of the University of Michigan's Center for Parallel Computing, which is part of the National Science Foundation's newly created National Partnership for Advanced Computing Infrastructure (NPACI).